Journal of Theoretical Biology 456 (2018) 62–73

Contents lists available at ScienceDirect

Journal of Theoretical Biology

journal homepage: www.elsevier.com/locate/jtb

Modeling of fusion inhibitor treatment of RSV in African green monkeys

Gilberto González-Parra[a,b], Hana M. Dobrovolny[a,*]

[a] Department of Physics & Astronomy, Texas Christian University, 2800 S University Dr. Fort Worth, TX 76129, USA
[b] Department of Mathematics, New Mexico Tech, Socorro, NM, USA

ARTICLE INFO

Article history:
Received 26 September 2017
Revised 18 April 2018
Accepted 22 July 2018
Available online 23 July 2018

Keywords:
Respiratory syncytial virus
Fusion inhibitors
African green monkey
Mathematical modelling
Drug efficacy

ABSTRACT

Respiratory syncytial virus (RSV) is a respiratory infection that can cause serious illness, particularly in infants. In this study, we test four different model implementations for the effect of a fusion inhibitor, including one model that combines different drug effects, by fitting the models to data from a study of TMC353121 in African green monkeys. We use mathematical modeling to estimate the drug efficacy parameters, ε_{max}, the maximum efficacy of the drug, and EC_{50}, the drug concentration needed to achieve half the maximum effect. We find that if TMC353121 is having multiple effects on viral kinetics, more detailed data, using different treatment delays, is needed to detect this effect.

© 2018 Elsevier Ltd. All rights reserved.

1. Introduction

Respiratory syncytial virus (RSV) infects the respiratory tract causing serious illness and death in infants and the elderly (Borchers et al., 2013). Since discovery of the virus in the 1950s (Chanock and Finberg, 1957; Chanock et al., 1957), researchers have been searching for an antiviral that can effectively slow or stop progression of the infection (Collins and Melero, 2011). There are a number of challenges in developing RSV antivirals including the short time course of the disease (Wright and Piedimonte, 2011), and the need for antivirals to be safe in infants and the elderly (Paes and Manzoni, 2011).

Treatment options for RSV are still very limited (Turner et al., 2014). Monoclonal antibodies are used prophylactically in high-risk infants (Forbes et al., 2014; Gutfraind et al., 2015), while ribavirin is used for treatment of very severe cases (Marcelin et al., 2014; Molinos-Quintana et al., 2013). Palivizumab is the most commonly used prophylactic therapy. It has been shown to reduce the incidence and the severity of RSV infections in infants (Andabaka et al., 2013; Frogel et al., 2008; Groothuis et al., 1993) and is associated with few adverse events (Chen et al., 2015). However, it does not prevent all RSV infections, does not seem to be particularly effective in treating the disease (Hu and Robinson, 2010; Rodriguez et al., 1997; Saez-Llorens et al., 2004), and can interfere with RSV diagnostic assays (Deming et al., 2013). Ribavirin is an antiviral used against a variety of viruses (Beaucourt and Vignuzzi, 2014) including RSV, although its effectiveness in treating RSV is not clear and is associated with safety concerns (Ventre and Randolph, 2007).

Recently, development of high-throughput screening methods (Kwanten et al., 2013; Lundin et al., 2013; Plant et al., 2015) and targeted design of drugs (Cancellieri et al., 2015; Cox and Plemper, 2016) has led to the development of new compounds that offer promise as RSV antivirals. Among the new compounds, there has been great interest in antivirals that target the RSV fusion protein (Sun et al., 2013). A number of fusion inhibitors have been identified (Andries et al., 2003; Bond et al., 2015; Bonfanti et al., 2008; Cianci et al., 2005; Feng et al., 2015; Lundin et al., 2010; Perron et al., 2016; Zheng et al., 2016), but with only one making it as far as clinical trials (DeVincenzo et al., 2014; Mackman et al., 2015). Among the discovered compounds, TMC353121 is a benzimidazole that was engineered to have a short half-life in tissue (Bonfanti et al., 2008), unlike its precursors (Bonfanti et al., 2007). TMC353121 has been shown to be effective in preventing fusion of RSV to the cell as well as preventing fusion of infected cells and uninfected cells (Roymans et al., 2010). Moreover, it has been tested in several animal models and reduces RSV viral load in cotton rats (Rouan et al., 2010), mice (Olszewska et al., 2011), and primates (Ispas et al., 2015).

Mathematical models can help in the transition of antiviral treatment to humans by optimizing treatment regimens and defining windows when treatment will be effective. Mathematical models have already been used to help guide treatment strategies for

* Corresponding author.
E-mail address: h.dobrovolny@tcu.edu (H.M. Dobrovolny).

https://doi.org/10.1016/j.jtbi.2018.07.029
0022-5193/© 2018 Elsevier Ltd. All rights reserved.

infectious diseases such as HIV (Perelson et al., 2012; Xiao et al., 2013), hepatitis (Canini and Perelson, 2014; Neumann et al., 1998), and influenza (Canini et al., 2014; Dobrovolny et al., 2011; Heldt et al., 2013). Similar strategies can be used to optimize treatment of RSV with fusion inhibitors. Since a recent study suggests that RSV fusion inhibitors share a common mechanism of action, we used TMC353121 as a tool compound to test different treatment strategies. To do so, we first needed to determine how to model the effect of TMC353121 as well as estimate the parameters that describe the efficacy of the antiviral. Since TMC353121 is a fusion inhibitor, essentially it should be modeled as changing parameters that govern the entry of the virus into the cell. There are several different ways to implement drug action for this type of antiviral (Beauchemin et al., 2008; Lou and Smith, 2011), and we need to determine which is most appropriate for RSV fusion inhibitors. We also need to determine two important drug efficacy parameters for TMC353121 before it can be accurately modeled: $\varepsilon_{\max}$ is the maximum possible effect of a drug, and EC_{50} is the drug concentration needed to achieve half the maximum effect. Note that both of these quantities depend on the effect we are measuring (Beggs and Dobrovolny, 2015), and in this case we need the values that quantify how the drug alters the parameters in our model.

In this paper, we use a recently described study of TMC353121 treatment of RSV infection in African green monkeys to extract drug efficacy parameters for TMC353121. We propose four mathematical implementations for the effect of the drug and examine how different drug models alter predicted disease time course. We use each of the four models to estimate the EC_{50} and $\varepsilon_{\max}$ for TMC353121 treatment in African green monkeys.

2. Methods

2.1. Model

In this study, we use a basic viral kinetics model (Baccam et al., 2006) given by the equations

$$\frac{dT}{dt} = -\beta TV \tag{1}$$

$$\frac{dE}{dt} = \beta TV - \frac{E}{\tau_E} \tag{2}$$

$$\frac{dI}{dt} = \frac{E}{\tau_E} - \frac{I}{\tau_I} \tag{3}$$

$$\frac{dV}{dt} = pI - cV \ . \tag{4}$$

In the model, target cells, T, become infected at rate β when they encounter virus, V. The cells then enter an eclipse phase, E, where they are not actively producing virus. After an average time τ_E, the cells move to the infectious phase I where they produce virus at a rate p. After an average time, τ_I, the cells die. Virus is cleared from the system at a rate c. Note that this model assumes exponential distributions for the transitions from eclipse to infectious and infectious to dead. While this is not as biologically realistic as other commonly-used models that assume other distributions for the transition times (Beauchemin et al., 2017; Holder and Beauchemin, 2011; Kakizoe et al., 2015; Pinilla et al., 2012), there is not enough data in these studies to properly parameterize a more complex model (Miao et al., 2011). We also do not include an explicit immune response due to the limited data in this study. The additional parameters needed to properly describe the immune response are not yet known and are not identifiable from the data available for this study. However, the effect of the immune response will be implicitly contained in the values of the parameter; we expect to have larger viral clearance and infectious cell death rates than in vitro due to the effect of antibodies and cytotoxic T cells, respectively.

2.2. Drug effect

We model the effect of an antiviral as reducing some model parameter by $1-\varepsilon$ where ε is the efficacy of the drug. ε ranges from 0 to 1 where 0 indicates the drug has no effect and 1 indicates that the drug is 100% effective. The drug efficacy can be related back to actual drug doses through the $E_{\max}$ model (Holford and Sheiner, 1981),

$$\varepsilon(t) = \varepsilon_{\max}\frac{C(t)^m}{C(t)^m + EC_{50}^m} \ , \tag{5}$$

where $C(t)$ is the drug concentration, $\varepsilon_{\max}$ is the maximum efficacy of the drug such that $0 < \varepsilon_{\max} \le 1$, EC_{50} is the concentration of drug necessary to inhibit the response by 50%, and m is the Hill coefficient. The Hill coefficient controls the steepness of the sigmoidal curve and is determined by the number of binding reactions needed for the drug to function (Weiss, 1997). Biochemical studies of TMC353121 suggest that it has a single binding site on the RSV fusion protein in its prefusion state (Battles et al., 2015), suggesting that an assumption of $m = 1$ is reasonable.

TMC353121 is a fusion inhibitor, so it prevents the virus from fusing with the cell membrane, thus preventing entry into the cell (Roymans et al., 2010). We test four possible implementations of the drug effect.

1. In the first implementation, we apply the drug effect to β in both the target (Eq. (1)) and eclipse (Eq. (2)) equations.
$$\frac{dT}{dt} = -(1-\varepsilon)\beta TV$$
$$\frac{dE}{dt} = (1-\varepsilon)\beta TV - \frac{E}{\tau_E}.$$
In this model, the infection is essentially just slowed since both removal from the target cells and entry into the eclipse phase are reduced simultaneously. We will refer to this implementation as the *slow infection* model.
2. In the second implementation, we apply the drug effect to β only in the eclipse equation (Eq. (2)).
$$\frac{dT}{dt} = -\beta TV$$
$$\frac{dE}{dt} = (1-\varepsilon)\beta TV - \frac{E}{\tau_E}.$$
In this case, target cells are removed from the system at a faster rate than eclipse cells appear. This essentially allows for some target cells to become protected from infection, reducing the available population of susceptible cells. We will refer to this implementation as the *protected target cell* or *protected T* model.
3. In the third implementation, the drug effect is applied to the duration of the eclipse phase, τ_E. In this case, we divide τ_E by $(1-\varepsilon)$ to lengthen the duration of the eclipse phase.
$$\frac{dE}{dt} = \beta TV - (1-\varepsilon)\frac{E}{\tau_E}$$
$$\frac{dI}{dt} = (1-\varepsilon)\frac{E}{\tau_E} - \frac{I}{\tau_I}$$
The interpretation here is that the drug causes an increase in the duration of the eclipse phase since it takes longer for the virus to actually enter the cell and begin the intracellular replication process. We will refer to the model as the *delayed production* model since the longer eclipse phase amounts to a delay in the production of virus. Note that for this model it is theoretically impossible to completely suppress the infection, since

cells are infected and will eventually transition to productively infectious.

4. Finally, we combine the delayed production and protected cell models to examine the possibility that TMC353121 has multiple effects.

$$\frac{dT}{dt} = -\beta TV$$
$$\frac{dE}{dt} = (1-\varepsilon)\beta TV - (1-\varepsilon)\frac{E}{\tau_E}$$
$$\frac{dI}{dt} = (1-\varepsilon)\frac{E}{\tau_E} - \frac{I}{\tau_I}$$

This is the *combination* model.

2.3. Experimental data

The experimental data for the treatment studies was taken from Ispas et al. (2015) and consists of two studies on African green monkeys. Both studies used a continuous infusion of TMC353121. The first study compared prophylactic treatment at a plasma level of 50 ng/mL with treatment started at 24 h post-infection, again at a plasma level of 50 ng/mL, and a control group. This study included 15 animals, 5 in each of the three groups. Starting 24 h post-infection, the control group received an infusion of 4% aqueous Captisol for 8 days. Starting 24 h before infection, the prophylactic group received an infusion of 0.033 mg/mL solution of TMC353121 at a flow rate of 2.5 mL/kg/h for 10 days. The treatment group received the same dose of TMC353121, but starting at 24 h post-infection for 8 days. All animals were followed until day 13 post-infection.

The second treatment study compared prophylactic treatment at two different plasma levels, 5 ng/mL and 500 ng/mL, with a control group. In this study, 12 animals were divided into the three groups. The control group again received an infusion of 4% aqueous Captisol starting 72 h before infection. The two prophylactic groups received infusions of a solution of 0.0033 mg/mL or 0.33 mg/mL of TMC353121 at a flow rate of 2.5 mL/kg/h , starting 72 h before infection. All groups were treated for 16 days and all animals were followed until 15 days post-infection.

For both studies, bronchoalveolar lavage fluid (BALF) was collected every two days from day 1 post-infection. RSV was quantified using one-Step RT-PCR. The threshold of detection for this method is 10^0 RNA/mL; viral loads lower than this value are recorded as 10^0 RNA/mL. Note that only the averaged results, as presented in Ispas et al. (2015), were used in this study.

2.4. Model fitting

To determine model parameters, we minimize the sum of squared residuals,

$$\mathrm{SSR} = \sum_{i=1}^{n} (y_i - f(t_i))^2, \tag{6}$$

where n is the number of experimental data points, y_i are the values of the experimental data points, and $f(t_i)$ are the model predictions at the times when experimental data were measured. To find the minimum, we used the `fmincon` function in Matlab which uses the interior-point algorithm to minimize a function subject to specified constraints. Data points that were below the threshold of detection contributed to the SSR only if the model prediction was above the threshold of detection (Baccam et al., 2006). For model comparison, we use the small-sample (second order) Akaike's "an information criterion" (AIC_C) for each fit using

$$\mathrm{AIC}_C = n\ln\left(\frac{SSR}{n}\right) + \frac{2(K+1)n}{n-K-2}, \tag{7}$$

where n is the number of data points and K is the number of parameters (Burnham and Anderson, 2002). Since the AIC_C imposes a penalty for additional parameters, the model with the lowest AIC_C is considered to be the better model given the experimental data.

We fit all three treatment groups within each study simultaneously, but fit each study separately. For the first study, we assumed that both the prophylactic and delayed treatment group had the same drug efficacy and that the infection in all three study arms could be described by the same infection parameters (p, β, c, τ_I, τ_E). Note that for this model, it is known that k, c, and δ are not separately identifiable (Smith et al., 2010) from viral titer measurements alone. Since this is a continuous infusion, we assumed that the drug efficacy remains constant over the course of the infusion. Measurements of plasma concentrations of TMC353121 during the study, as shown in Fig. 1 of Ispas et al. (2015) suggest that this is a reasonable approximation. For the second study, we again assumed that all three study arms are described by the same base infection parameters, possibly different from those of study 1. Since we have different drug concentrations in this study, we apply the $E_{\max}$ model and fit both $\varepsilon_{\max}$ and EC_{50}. We use the target plasma concentrations as the constant amount of drug in Eq. (5). For both studies, we assume that infection is initiated with an initial viral inoculum (to be determined from fitting). We set the initial number of target cells to 1 and the initial number of eclipse and infectious cells to 0. Bootstrapping is used to determine the 95% confidence intervals.

In addition to estimating drug efficacy and infection parameters, we use our model fits to calculate two additional quantities of interest. The infecting time, given by $t_{\mathrm{inf}} = \sqrt{2/p\beta}$, is the time between release of a virion from an infected cell and infection of the next cell. The basic reproductive number, $R_0 = p\beta\tau_I/c$, is the number of secondary infections resulting from the introduction of a single infected cell into a homogeneous susceptible population. Both of these quantities give a measure of how quickly the infection spreads.

3. Results

3.1. Modeling of fusion inhibitors

We first examine three different possible single effect models for an RSV fusion inhibitor. Before testing the models using experimental data, it is useful to compare their predictions of the effect of a fusion inhibitor. Here, we use the same $\varepsilon_{\max}$ for all models ($\varepsilon_{\max}$=0.95) and use a drug concentration measured relative to EC_{50} ($D \longrightarrow D/\mathrm{EC}_{50}$). We use parameter values found from fitting the model to data from study 2 (discussed in Section 3.3.2). While there are previous estimates of some of these parameters for in vivo RSV infections (González-Parra and Dobrovolny, 2015), a different model was used for these, so we do not have a complete set of parameters for our model. Fig. 1 shows the predicted time course of treated infections for the three models assuming different treatment delays at three different drug concentrations. The slow infection and protected target cell models make similar predictions of the effect of treatment, although there are measurable differences in the time courses when the treatment delay is near 6 d and the drug concentration is near EC_{50}. When the drug concentration is high, these differences in predicted viral time course disappear. The delayed production model gives quite different predictions. While the slow infection and protected target cell models predict suppression of the infection at these drug concentrations, the delayed production model predicts continued growth.

A more detailed study of this effect is shown in Fig. 2 where we plot the change in duration of the infection (time spent above 10^1, a typical virus detection level) as a function of drug concentration relative to EC_{50} and treatment delay. In these figures, yellow indi-

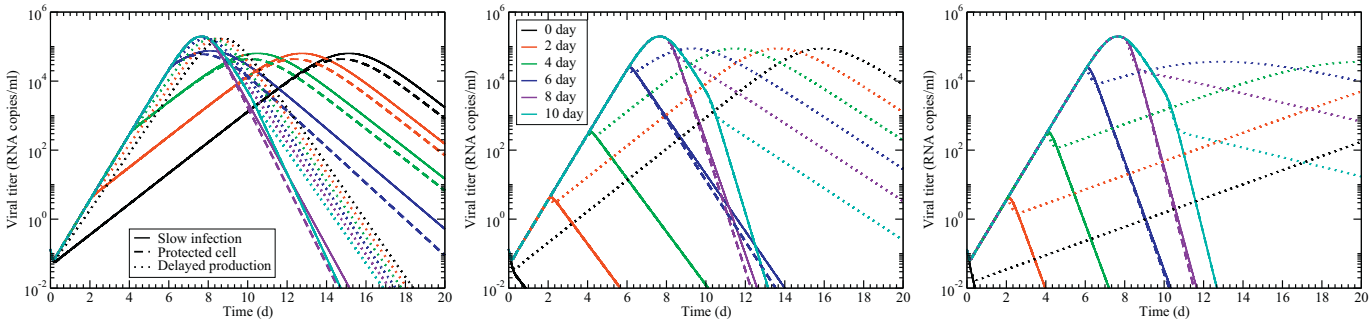

Fig. 1. Model predictions of treatment outcomes if treatment is applied after the onset of infection. The drug is assumed to have the same maximum effect ($\varepsilon_{max} = 0.95$) and is applied at concentrations of 0.5 times EC_{50} (left), 5 times EC_{50} (center), and 50 times the EC_{50} (right). The slow infection model predictions are given by solid lines, the protected target cell model predictions are given by dashed lines, and the delayed production model predictions are given by dotted lines. Different colors correspond to different times of treatment initiation as indicated in the legend of the center graph.

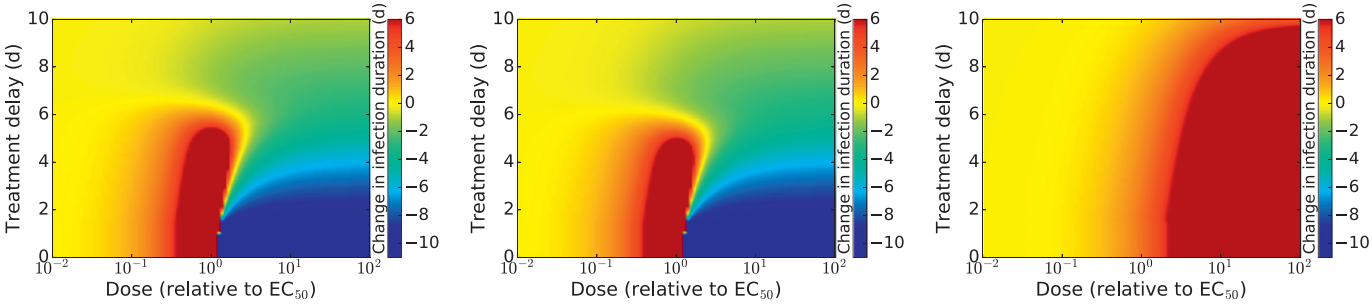

Fig. 2. Model predictions of change in infection duration as a function of drug concentration and treatment delay for the slow infection model (left), the protected target cell model (center), and the delayed production model (right) assuming an ε_{max} of 0.95. A negative change indicates that the infection is shortened by application of the drug, while a positive change indicates that the infection duration is lengthened by the drug.

cates that application of the drug does not change the duration of the infection, while blue/green (negative values) indicate a shortening of the infection in the presence of antiviral and orange/red indicates a lengthening of the infection in the presence of antiviral. Here it is difficult to see the slight differences in the predictions between the slow infection and protected target cell models, but the delayed production model gives drastically different predictions. For the slow infection and protected target cell models, there is a range of doses and treatment delays that lead to a longer-lasting infection than without treatment. This region occurs at drug doses near and somewhat below the EC_{50} with treatment delays up to about 6 d. If we use higher doses of antiviral, then treatment shortens the duration of the infection, but only if treatment is started before $\sim$5 days post-infection. The delayed production model, however, predicts that higher doses of antivirals will lengthen the infection; there is no dose or time delay that would lead to a shortening of the infection.

3.2. Combining mechanisms of action

While the delayed production model on its own appears to be a poor model choice, it's possible that TMC353121 could have multiple effects. For example, the drug could protect some cells from infection, and for the cells still susceptible to infection, it could interfere with the fusion process delaying production of new virions. Here, we examine a model with these combined effects. Note that combining the slow infection and the delayed production models leads to similar results (not shown). Fig. 3 shows predictions of viral titer time courses and infection duration for the model combining protected target cell and delayed production effects. Combining the two models leads to greater suppression of growth of the infection than with just the protected target cell model alone. While infection growth might be slower, this does not necessarily result in many changes in the duration of the infection. The combined model predicts changes in infection duration similar to the protected target cell model over many doses and treatment delays. You would only notice that the antiviral delays production in addition to protecting cells from infection if you treat with doses over the EC_{50} with treatment delays of 4–10 days.

3.3. Fitting models to experimental data

3.3.1. Study 1

To determine which model is the most appropriate for modeling of TMC353121, the models were fit to experimental data from two studies in African green monkeys. Model fits and parameter estimates for Study 1 are presented in Fig. 4. All four models fit the data of the treated groups well, but have trouble capturing the peak viral titer of the control group in favor of more accurately capturing other data points. All four assumptions for the mechanism of action of the fusion inhibitor will cause viral peak to shift to the right as the drug concentration increases. While the experimental data shows a slightly shifted peak for the prophylactic group, the peak for the delayed treatment group occurs at almost the same time as the peak for the control group. The models predict that the peak for the treatment group occurs between 6–23 h before the peak of the prophylactic group. Since viral titer is measured experimentally every two days, such a small shift in peak viral titer is not captured very accurately. Additionally, if we assume that the two day sampling frequency leads to a time measurement error of ± 1 days, then the shift in time of peak between control and prophylactic can be anywhere from 0–4 days, a wide range that includes predictions from all four models. In this study, the model that assumes the drug protects some target cells produces a slightly lower AIC_C, making it the better choice for explaining these experimental results.

All four models produce similar estimates for the infection parameters. The average duration of the eclipse phase and the

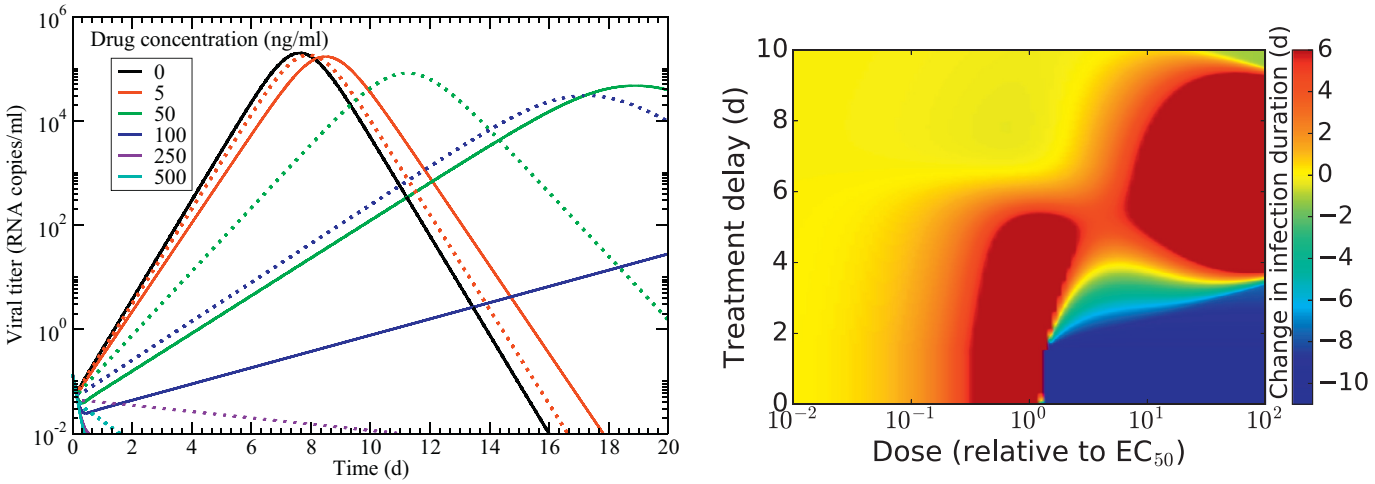

Fig. 3. Predictions of a model combining protected target cells and delayed production. (left) Predicted viral titers of the combined model are shown for several different drug concentrations (solid lines). For comparison, dotted lines show the predictions of only the protected target cell model. (right) Change in the duration of the infection as dose and treatment delay are varied for the combined model.

average infectious lifespan are 12–15 h, with the exception of the estimated eclipse duration for the delayed production model which estimates that the duration of the eclipse phase is only 0.27 h. The clearance rate here is somewhat larger than previously estimated for in vitro systems (González-Parra et al., 2018) (0.08/h vs. 0.04/h), perhaps reflecting the effect of the immune response in the monkeys. It is, however, lower than the clearance rate of 0.20 /h estimated in humans (González-Parra and Dobrovolny, 2015). The infecting time is estimated to be between 3 and 6 h which is slightly longer than the estimated $\sim$2 h for humans (González-Parra and Dobrovolny, 2015) and 3 h for in vitro infections (González-Parra et al., 2018).

The models vary quite widely in their estimates of the efficacy of the drug at a plasma concentration of 50 ng/mL, giving a 28% efficacy for the slow infection model, a 57% efficacy for the protected T model, a 90% efficacy for the delayed production model, and a 25% efficacy for the combined model.

3.3.2. Study 2

Model fits and parameter estimates for Study 2 are presented in Fig. 5. All three models fit the data from the treatment groups well, resulting in similar SSRs and AIC_C. Note that for the 500 ng/mL treatment arm, all points are at the level of detection, so model predictions with viral titers lower than the threshold are consistent with the experimental data. The estimated average infectious durations here are $\sim$3–4 h, somewhat shorter than previous estimates of 9 h and 12 h (González-Parra et al., 2018; González-Parra and Dobrovolny, 2015). Similarly, the duration of the eclipse phase ($\sim$3–4 h) is also shorter than previous estimates of 6 h and 14 h (González-Parra et al., 2018; González-Parra and Dobrovolny, 2015). The infecting times are estimated here at $\sim$3 h, which is similar to previous estimates (González-Parra et al., 2018; González-Parra and Dobrovolny, 2015). The clearance rate is large for this study (0.2–0.3 /h), more in line with the estimated clearance rate in humans (González-Parra and Dobrovolny, 2015). The basic reproductive number is slightly larger than 1, suggesting an infection that does not spread very quickly. Note that there are some differences in the control data for the two studies, with the control from Study 2 having a lower viral titer peak and a later time of peak viral titer than Study 1. Thus, it is not entirely surprising that the parameters describing these infections differ. Here, the protected T model and the combination model both have the lowest AIC_C, suggesting that it is impossible to differentiate between the two models with the current data set.

The four models estimate different maximum drug efficacies ranging from 63–100% and also give different estimates of the EC_{50} (157 ng/mL for the slow infection model, 149 ng/mL for the protected target cell model, 22.4 ng/mL for the delayed production model, and 141 ng/mL). The EC_{50} for TMC353121 in HeLa cells was found to be 0.07 ng/mL (Bonfanti et al., 2008), but was much larger, 200 ng/mL, and closer to the values found here, in cotton rats (Rouan et al., 2010).

3.3.3. Model treatment predictions

The different ε_{max} and EC_{50} translate into differences in predicted drug efficacies for the three models as shown in Fig. 6. For any drug concentration, the delayed production model results in the highest efficacy both because it has a higher possible maximum effect, but also because it has a lower EC_{50}. Note that the maximum efficacy here refers to the maximum possible reduction in the infection rate (or increase in eclipse duration) during an in vivo infection, which is different from the drug's efficacy in reducing viral titers. We have also indicated the efficacies estimated by fits to study 1 for a 50 ng/mL dose. There is not particularly good agreement between the two estimates, with study 1 overestimating the efficacy predicted by the results of study 2. This might be, in part, due to differences in the control data between the two studies. The control data from study 1 has a higher peak viral titer than the control data from study 2, so it's not surprising that a higher efficacy would be needed to reduce the viral load.

These differences in the predicted efficacy lead to differences in predictions of the viral time courses at different drug concentrations. Fig. 7 shows the model predictions for a few different drug concentrations under continuous infusion and prophylactic treatment. The slow infection and protected target cell models lead to very similar outcomes at most drug concentrations. The most noticeable difference occurs at a drug concentration of 250 ng/mL (purple line). At this drug concentration, the protected target cell model shows clear decay of viral load, but the slow infection model has a viral load that appears almost constant. There is a more stark difference in model predictions between these two models and the delayed production or combination models. Interestingly, even though the delayed production model predicts higher efficacies for any given drug concentration, this does not translate into better effectiveness at reducing viral load. While the model predicts that TMC353121 is very effective at increasing the duration of the eclipse phase, this does not translate into efficient reduction of viral load nor does it agree well with experimental

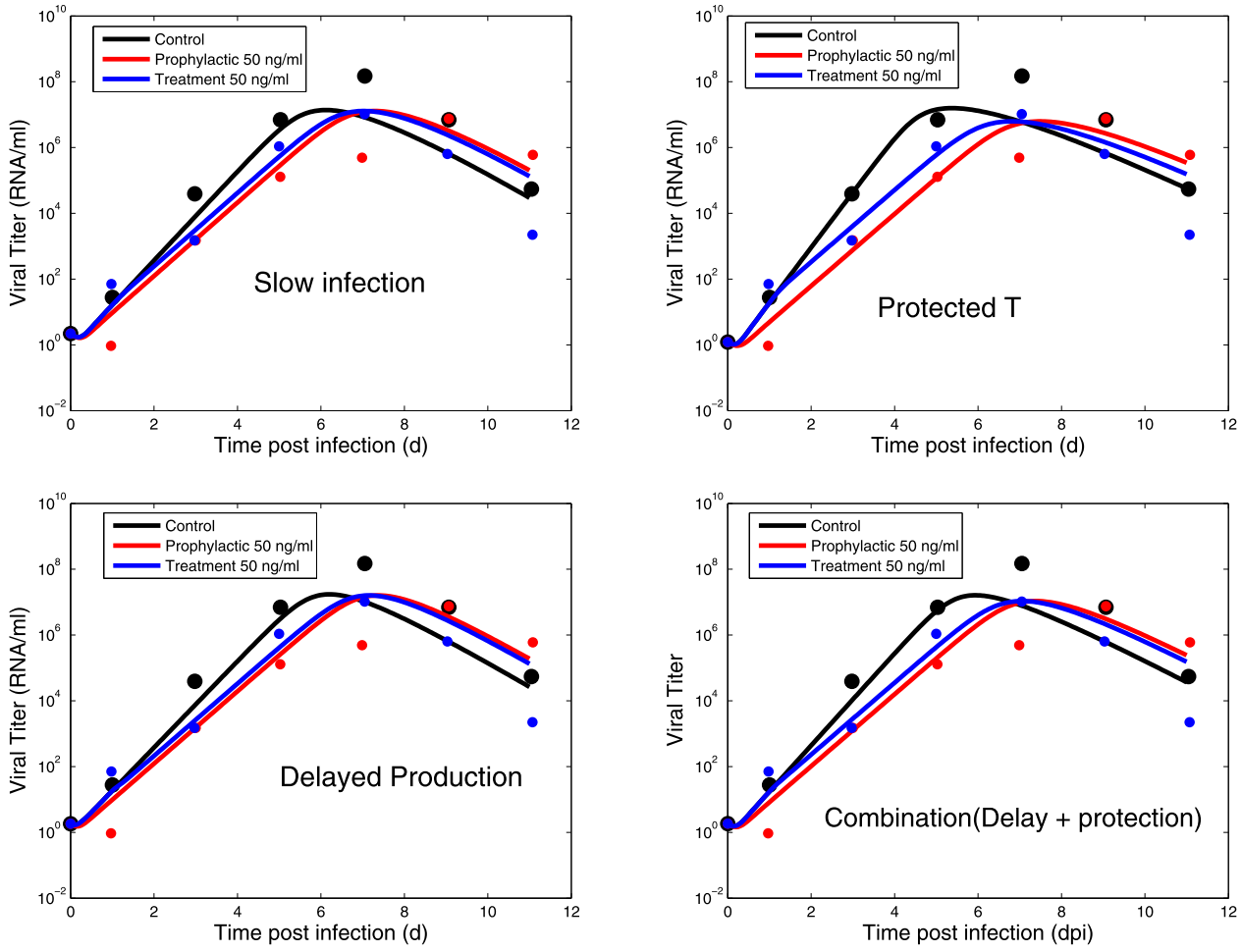

Parameter	p ((RNA/mL)/(h · cell))	β ((RNA/mL)$^{-1}$ · h^{-1})	t_{inf} (h)
Slow Infection	5.08×10^{6} $(1.32–45.1)\times10^{6}$	2.32×10^{-8} $(0.319–10.1)\times10^{-8}$	4.21 (0.653–21.8)
Protected T	4.25×10^{6} $(1.03–118)\times10^{6}$	4.21×10^{-8} $(0.211–16.3)\times10^{-8}$	3.34 (0.323–30.3)
Delayed Production	5.25×10^{6} $(1.35–47.0)\times10^{6}$	8.33×10^{-9} $(1.57–25.7)\times10^{-8}$	6.76 (1.29–30.7)
Combination	3.96×10^{6} $(1.11–45.0)\times10^{6}$	1.75×10^{-8} $(0.282–4.71)\times10^{-8}$	5.37 (0.969–25.2)
Parameter	c (/h)	τ_I (h)	τ_E (h)
Slow Infection	0.0863 (0.0579–0.140)	12.0 (6.51–18.4)	12.2 (6.42–18.8)
Protected T	0.0704 (0.0386–0.559)	15.4 (1.10–30.5)	15.0 (0.417–30.5)
Delayed Production	0.0775 (0.0527–0.133)	12.0 (6.76–18.2)	0.271 (0.0887–0.721)
Combination	0.0750 (0.0554–0.132)	15.2 (7.48–21.3)	4.90 (3.56–7.36)
Parameter	V_0 (RNA/mL)	ε	R_0
Slow Infection	2.20 (0.335–18.9)	0.284 (0.111–0.410)	16.4 (0.196–1490)
Protected T	1.21 (0.211–16.4)	0.568 (0.103–0.625)	39.1 (0.00428–15200)
Delayed Production	1.82 (0.311–11.3)	0.895 (0.810–0.929)	6.77 (0.108–415)
Combination	1.84 (0.155–2.15)	0.253 (0.289–0.0550)	14.0 (0.178–820)
Parameter	SSR	AIC_C	
Slow Infection	10.8 (3.28–15.4)	14.0 (-11.0–21.5)	
Protected T	9.14 (1.76–13.1)	10.5 (-24.1–18.1)	
Delayed Production	10.9 (3.58–16.4)	14.2 (-9.15–22.8)	
Combination	10.3 (3.67–16.4)	13.0 (-8.62–22.9)	

Fig. 4. Model fits and parameter estimates for Study 1 assuming that TMC353121 slows the infection (top left), protects target cells (top right), delays production (bottom left), or has a combined effect (bottom right). Experimental data is the mean $\log_{10}$ viral load of measurements from animals in each group.

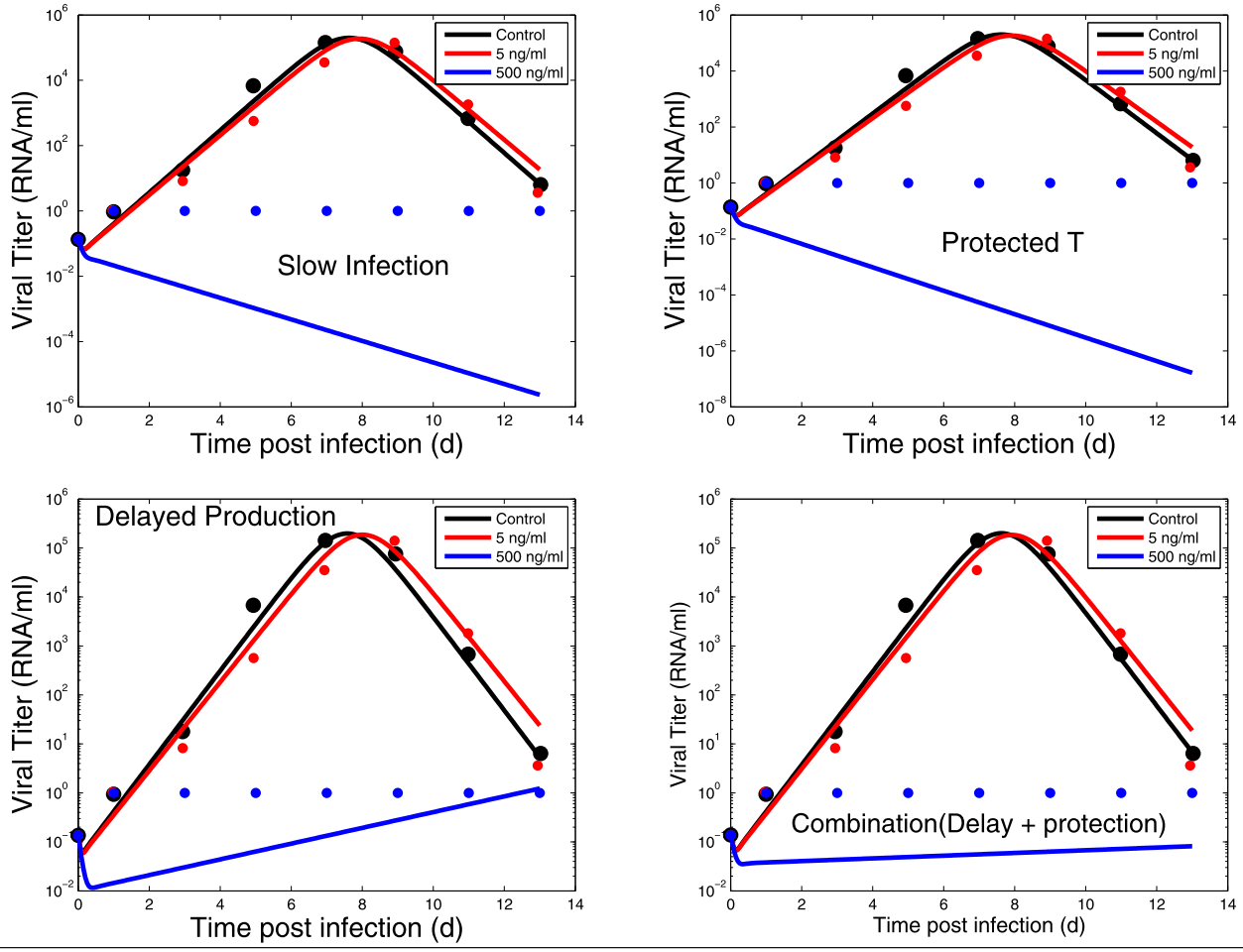

Parameter	p ((RNA/mL)/(h · cell))	β ((RNA/mL)$^{-1}$ · h^{-1})	t_{inf} (h)
Slow Infection	1.03×10^{6} (0.455–2.31)$\times10^{6}$	2.02×10^{-7} (1.07–4.08)$\times10^{-7}$	3.10 (1.45–6.35)
Protected T	9.47×10^{5} (3.66–19.4)$\times10^{5}$	2.10×10^{-7} (1.11–4.32)$\times10^{-7}$	3.17 (1.54–7.02)
Delayed Production	4.31×10^{5} (0.00878–27.3)$\times10^{5}$	3.16×10^{-7} (0.437–1720)$\times10^{-7}$	3.83 (0.0653–228)
Combination	1.27×10^{6} (0.593–3.22)$\times10^{6}$	1.83×10^{-7} (0.840–3.64)$\times10^{-7}$	2.93 (1.31–6.34)
Parameter	c (/h)	τ_I (h)	τ_E (h)
Slow Infection	0.312 (0.240–0.380)	3.22 (2.43–4.14)	3.13 (2.35–4.03)
Protected T	0.300 (0.227–0.375)	3.35 (2.61–4.49)	3.32 (2.52–4.39)
Delayed Production	0.217 (0.111–4.12)	4.33 (3.40–11.2)	4.00 (0.235–21.3)
Combination	0.337 (0.280–0.416)	2.94 (2.42–3.52)	2.87 (2.34–3.42)
Parameter	V_0 (RNA/mL)	$\varepsilon_{\max}$	EC_{50} (ng/mL)
Slow Infection	0.135 (0.0502–0.342)	0.871 (0.551–0.871)	157 (47.1–263)
Protected T	0.138 (0.0551–0.321)	0.918 (0.585–0.918)	149 (47.8–301)
Delayed Production	0.146 (6.59×10^{-4}–69.6)	1.00 (0.892–1.00)	22.4 (1.01–986)
Combination	0.139 (0.0527–0.317)	0.632 (0.499–0.722)	141 (46.0–170)
Parameter	R_0	SSR	AIC_C
Slow Infection	2.15 (0.316–16.3)	1.74 (0.561–2.30)	-32.1 (-59.3– -25.4)
Protected T	2.22 (0.282–16.6)	1.73 (0.681–2.43)	-32.3 (-54.6– -24.1)
Delayed Production	2.72 (3.17×10^{-6}–47400)	1.95 (0.315–2.48)	-29.4 (-73.1– -23.6)
Combination	2.03 (0.290–14.7)	1.73 (0.579–2.18)	-32.3 (-58.5– -26.7)

Fig. 5. Model fits and parameter estimates for Study 2 assuming that TMC353121 slows the infection (left), protects target cells (center), or delays production (right). Experimental data is the mean $\log_{10}$ viral load of measurements from animals in each group.

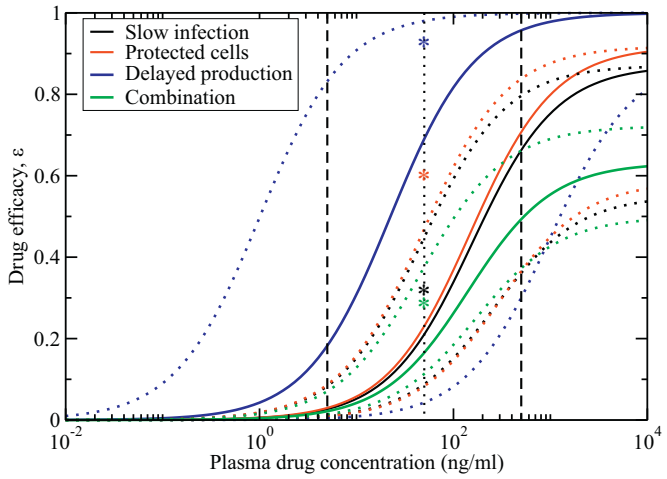

Fig. 6. Model predictions of the efficacy of prophylactic treatment with TMC353121 for the second study. Solid lines show the efficacy curves produced by the estimates of ε_{max} and EC_{50} from Study 2. Dotted lines show the 95% confidence intervals. The vertical dashed lines indicate the drug concentrations used in study 1 and study 2 (5, 50, and 500 ng/mL). The '*' indicates the efficacies estimated in the fits to study 1.

treatment data. None of the drug concentrations examined here lead to clearance of the infection according to the delayed production model. The combination model differs from the slow infection and protected cell models primarily at high doses of drug, where the addition of the second mechanism leads to long-lasting infections.

For the slow infection and protected target cells, we can predict the amount of drug needed to suppress the infection under the assumption of prophylactic treatment. The minimum drug efficacy that leads to suppression is given by Dobrovolny et al. (2011)

$$\varepsilon_{min} = 1 - \frac{1}{R_0}, \tag{8}$$

where R_0 is the basic reproductive number and is given by Baccam et al. (2006)

$$R_0 = \frac{p\beta T_0 \tau_I}{c}. \tag{9}$$

Using the parameters given in Fig. 5, we find the minimum efficacies to be 0.53 for the slow infection model and 0.55 for the protected target cell model. We can then use Eq. (5) to find the corresponding drug concentration. For the slow infection model, we find the drug concentration needed to suppress the infection is 249 ng/mL while for the protected target cell model, we find the concentration needed to suppress the infection is 222 ng/mL. This explains the differences observed in the 250 ng/mL curves of Fig. 7, since this concentration is barely enough to suppress the infection in the slow infection model, but somewhat more than what is needed to suppress the infection in the protected target cell model.

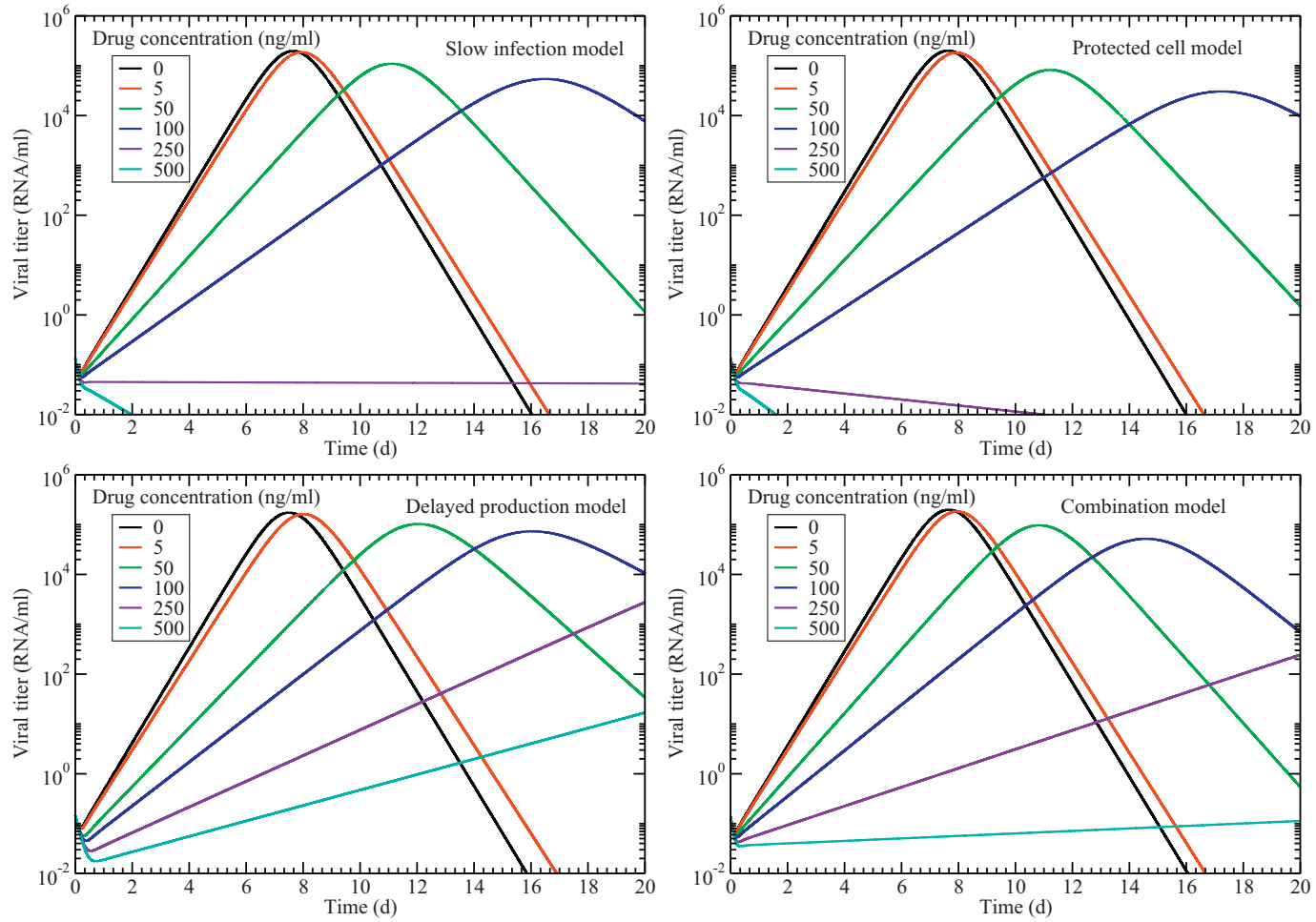

Fig. 7. Model predictions of treatment outcomes at different drug concentrations. We assume prophylactic treatment at a constant drug concentration using the slow infection model (top left), the protected target cell model (top right), the delayed production model (bottom left), and the combination model (bottom right).

4. Discussion

In this paper, we examined different possible implementations for modeling the effect of RSV fusion inhibitors as exemplified by applying TMC353121. While we used TMC353121 in this study, many of our results are likely applicable for other RSV fusion inhibitors (Bond et al., 2015; Feng et al., 2015; Lundin et al., 2010; Perron et al., 2016; Zheng et al., 2016) which have similar mechanisms of action. We found that all four proposed models fit the experimental data almost equally well, suggesting that more detailed experiments will be needed to differentiate between different models. Our examination of the combined model suggests that if a fusion inhibitor delays production in addition to protecting cells, the effect of the delayed production is most apparent at treatment delays not yet examined in experiment. This could have serious implications if fusion inhibitors move to broad use in patients. Challenge studies suggest that RSV symptoms appear 2–4 days post infection (Bagga et al., 2013; DeVincenzo et al., 2015; 2010) and it might take another day or two for patients to get in to their doctor and get a prescription. It is not unreasonable, then, to assume that there might be delays of 4–6 days before treatment is initiated. This would put the patient in the range where the protected target cell model and the combined model differ drastically in their predictions. If a fusion inhibitor does not change the duration of the eclipse phase, then the patient will reduce the duration of their infection by taking this drug, but if the fusion inhibitor has an effect on the duration of the eclipse phase, then the patient will actually lengthen the duration of the infection with treatment. In vivo experiments with a longer time delay before initiation of treatment would help ensure that such surprises do not appear as treatment is tested in humans.

We also extracted the maximum efficacy ($\varepsilon_{\max}$) and the drug concentration required to achieve half the maximum effect (EC_{50}) for all four models. $\varepsilon_{\max}$ has not previously been measured for this antiviral, but we found that it was fairly high (over 63%) for all three models. The EC_{50} has been previously measured for this antiviral, both in vitro (Bonfanti et al., 2008) and in vivo in cotton rats (Rouan et al., 2010). Our estimates of EC_{50} are close to the value found in cotton rats, but substantially larger than the value found in vitro. There are several possible reasons for this difference. Several antivirals have been shown to result in different EC_{50}s when tested in different cell lines (Hazen and Lanier, 2003; Leary et al., 2002; Smee et al., 2007). There is also evidence that the measured EC_{50} is dependent on the initial viral inoculum (Ståhle et al., 1998; Wildum et al., 2013), which is likely different in vitro and in vivo. Another possibility is that during the course of an infection, mutant strains resistant to the effect of the antiviral could arise (Aljabr et al., 2016; Yan et al., 2014), driving the EC_{50} to higher values. Additionally, measurement of antiviral concentrations in plasma might not be reflective of antiviral availability within the respiratory tract (Gonzalez et al., 2013), giving an incorrect measure of the EC_{50}. Finally, experimental error in viral titer measurements (LaBarre and Lowy, 2001) and issues with repeatability (Paradis et al., 2015) will affect estimates of all of these parameters. This is seen quite clearly here in the lack of agreement between drug efficacy estimates between Study 1 and Study 2, possibly driven, in part, by inconsistencies in the control data between the two studies.

It should be stressed that $\varepsilon_{\max}$ and EC_{50} depend on what is being measured (Beggs and Dobrovolny, 2015; Weinberg et al., 2007). This is seen quite clearly for the delayed production model. For this model, we estimated an $\varepsilon_{\max}$ of 1.0, but this was with respect to the antivirals effect on changing the duration of the eclipse phase. If we had used the duration of the infection as a measured endpoint, we would have concluded that the antiviral was completely ineffective. Thus, the $\varepsilon_{\max}$ and EC_{50} estimated here are the parameters needed to implement the mathematical models which we can then use to run simulations that can extract $\varepsilon_{\max}$ and EC_{50} for other endpoints of interest such as reduction in viral titer or reduction in infection duration.

While RSV replicates easily in the AGM model (Taylor, 2017; Weiss et al., 2003), the animals exhibit few clinical symptoms (Ispas et al., 2015; Jones et al., 2012; Kakuk et al., 1993), so they do not completely reproduce the infection dynamics of humans. There are also differences in the immune response of AGM and humans (Kahn et al., 2011), which will cause differences in disease dynamics in the two hosts. This can have consequences for translating antiviral use from AGM to humans, as has been observed in some vaccine studies (Graham, 2011). Thus we should be cautious about extrapolating some of the details of these results to humans.

Our model fits to data from Study 2 were better than our model fits to Study 1. Ideally, a single model should be able to accurately reproduce both studies. While this could indicate that none of the models are correctly capturing the effect of a fusion inhibitor, the poorer fit to Study 1 is reasonable when experimental error is taken into consideration. As mentioned earlier, given the 2 days sampling frequency, a reasonable assumption for error in any time measurements is $\pm$1day. Estimates of measurement error in viral load measured by qRT-PCR are ± 1.0 log RNA/mL (Hayden et al., 2015; Hoffman et al., 2008; Sedlak et al., 2017), consistent with the discrepancy in peak viral titer of the two control arms. Within these error estimates, the fits of Study 1 are consistent with the experimental data, so we cannot be certain that a refined model is necessary. Further experiments that sample viral load more frequently to reduce the error in time or that include more animals to reduce the error in viral titer measurements will help clarify whether a new antiviral model is needed.

This model also does not include an explicit immune response, although the effect of the immune response is reflected in the estimated values of some parameters. For example, we consistently found that the clearance rate in AGM is higher than in vitro (González-Parra et al., 2018), most likely reflecting the effect of antibodies. The exact mathematical formulation for different components of the immune response is still unclear (Dobrovolny et al., 2013; Eftimie et al., 2016; Pawelek et al., 2012). This coupled with the additional parameters needed for describing the immune response make it difficult to include these details in this study. Unfortunately, choice of model (Cao and McCaw, 2017; Dobrovolny et al., 2010; Liao et al., 2017), particularly inclusion of an immune response (Cao and McCaw, 2017), can alter the predicted outcome of antiviral treatment. More detailed experiments, including measurements of the immune response, will help in the development of more accurate models of antiviral treatment.

There are other limitations in using this particular viral kinetics model. As previously mentioned, this model does not model transitions from eclipse to infectious and infectious to dead accurately (Holder and Beauchemin, 2011), although this is most apparent in trying to reproduce the results of single cycle experiments. We also assumed that the Hill coefficient for the drug effect is 1. While we believe this is the case for TMC353121, this might not be the case for all RSV fusion inhibitors. Studies indicate that a Hill coefficient not equal to 1 will alter the predicted efficacy of antiviral treatment (Chang et al., 2016; Sampah et al., 2011). Finally, this viral kinetics model does not describe the fusion process in detail, limiting our description of the drug effect. While some more detailed models for viral entry have been proposed (Dee et al., 1995; Dee and Shuler, 1997; Schelker et al., 2016; Sidorenko and Reichl, 2004), none of these are specifically for RSV, and they contain too many parameters for the limited data used here. Nonetheless, our model has highlighted a possible deficiency of treatment studies of fusion inhibitors that should be corrected in future experiments.

Acknowledgments

The authors would like to acknowledge the assistance and helpful advice provided by Gabriela Ispas, Filip De Ridder, Dymphy Huntjens, and Dirk Roymans. Hana M. Dobrovolny received funding from Janssen Research and Development Belgium, and Gilberto Gonzalez-Parra's salary was paid by a grant from Janssen R&D Belgium [grant number 610765].

References

Aljabr, W., Touzelet, O., Pollakis, G., Wu, W., Munday, D.C., Hughes, M., Hertz-Fowler, C., Kenny, J., Fearns, R., Barr, J.N., Matthews, D.A., Hiscox, J.A., 2016. Investigating the influence of ribavirin on human respiratory syncytial virus RNA synthesis by using a high-resolution transcriptome sequencing approach. J. Virol. 90 (10), 4876–4888. doi:10.1128/JVI.02349-15.

Andabaka, T., Nickerson, J.W., Rojas-Reyes, M.X., Rueda, J.D., Vrca, V.B., Barsic, B., 2013. Monoclonal antibody for reducing the risk of respiratory syncytial virus infection in children. Cochrane Database Syst. Rev. 4. doi:10.1002/14651858.CD006602.pub4. UNSP CD006602

Andries, K., Moeremans, M., Gevers, T., Willebrords, R., Sommen, C., Lacrampe, J., Janssens, F., Wyde, P.R., 2003. Substituted benzimidazoles with nanomolar activity against respiratory syncytial virus. Antiviral Res. 60 (3), 209–219. doi:10.1016/j.antiviral.2003.07.004.

Baccam, P., Beauchemin, C., Macken, C.A., Hayden, F.G., Perelson, A.S., 2006. Kinetics of influenza a virus infection in humans. J. Virol. 80 (15), 7590–7599. doi:10.1128/JVI.01623-05.

Bagga, B., Woods, C.W., Veldman, T.H., Gilbert, A., Mann, A., Balaratnam, G., Lambkin-Williams, R., Oxford, J.S., McClain, M.T., Wilkinson, T., Nicholson, B.P., Ginsburg, G.S., DeVincenzo, J.P., 2013. Comparing influenza and RSV viral disease dynamics in experimentally infected adults predicts clinical effectiveness of RSV antivirals. Antivir. Ther. 18, 785–791. doi:10.3851/IMP2629.

Battles, M.B., Langedijk, J.P., Furmanova-Hollenstein, P., Chaiwatpongsakorn, S., Costello, H.M., Kwanten, L., Vranckx, L., Vink, P., Jaensch, S., Jonckers, T.H.M., Koul, A., Arnoult, E., Peeples, M.E., Roymans, D., McLellan, J.S., 2015. Molecular mechanism of respiratory syncytial virus fusion inhibitors. Nat. Chem. Biol. 12 (2), 87–95. doi:10.1038/NCHEMBIO.1982.

Beauchemin, C.A.A., McSharry, J.J., Drusano, G.L., Nguyen, J.T., Went, G.T., Ribeiro, R.M., Perelson, A.S., 2008. Modeling amantadine treatment of influenza a virus in vitro. J. Theor. Biol. 254, 439–451. doi:10.1016/j.jtbi.2008.05.031.

Beauchemin, C.A.A., Miura, T., Iwami, S., 2017. Duration of SHIV production by infected cells is not exponentially distributed: implications for estimates of infection parameters and antiviral efficacy. Sci. Rep. 7, 42765. doi:10.1038/srep42765.

Beaucourt, S., Vignuzzi, M., 2014. Ribavirin: a drug active against many viruses with multiple effects on virus replication and propagation. molecular basis of ribavirin resistance. Curr. Opin. Virol. 8, 10–15. doi:10.1016/j.coviro.2014.04.011.

Beggs, N.F., Dobrovolny, H.M., 2015. Determining drug efficacy parameters for mathematical models of influenza. J. Biol. Dyn. 9 (S1), 332–346. doi:10.1080/17513758.2015.1052764.

Bond, S., Draffan, A.G., Fenner, J.E., Lambert, J., Lim, C.Y., Lin, B., Luttick, A., Mitchell, J.P., Morton, C.J., Nearn, R.H., Sanford, V., Stanislawski, P.C., Tucker, S.P., 2015. The discovery of 1,2,3,9b-tetrahydro-5h-imidazo[2,1-a]isoindol-5-ones as a new class of respiratory syncytial virus (RSV) fusion inhibitors. part 1. Bioorg. Med. Chem. Lett. 25 (4), 969–975. doi:10.1016/j.bmcl.2014.11.018.

Bonfanti, J.-F., Doublet, F., Fortin, J., Lacrampe, J., Guillemont, J., Queguiner, P.M.L., Arnoult, E., Gevers, T., Janssens, P., Szel, H., Willebrords, R., Timmerman, P., Wuyts, K., Janssens, F., Sommen, C., Wigerinck, P., Andries, K., 2007. Selection of a respiratory syncytial virus fusion inhibitor clinical candidate, part 1: improving the pharmacokinetic profile using the structure-property relationship. J. Med. Chem. 50 (19), 4572–4584. doi:10.1021/jm070143x.

Bonfanti, J.-F., Meyer, C., Doublet, F., Fortin, J., Muller, P., Queguiner, L., Gevers, T., Janssens, P., Szel, H., Willebrords, R., Timmerman, P., Wuyts, K., van Remoortere, P., Janssens, F., Wigerinck, P., Andries, K., 2008. Selection of a respiratory syncytial virus fusion inhibitor clinical candidate. 2. discovery of a morpholinopropylaminobenzimidazole derivative (TMC353121). J. Med. Chem. 51 (4), 875–896. doi:10.1021/jm701284j.

Borchers, A.T., Chang, C., Gershwin, M.E., Gershwin, L.J., 2013. Respiratory syncytial virus—a comprehensive review. Clin. Rev. Allergy Immunol. 45 (3), 331–379. doi:10.1007/s12016-013-8368-9.

Burnham, K.P., Anderson, D.R., 2002. Model Selection and Multimodel Inference: A Practical Information-Theoretic Approach, second Springer-Verlag New York Inc., New York, USA.

Cancellieri, M., Bassetto, M., Widjaja, I., van Kuppeveld, F., de Haan, C.A.M., Brancale, A., 2015. In silico structure-based design and synthesis of novel anti-RSV compounds. Antiviral Res. 122, 46–50. doi:10.1016/j.antiviral.2015.08.003.

Canini, L., Conway, J.M., Perelson, A.S., Carrat, F., 2014. Impact of different oseltamivir regimens on treating influenza a virus infection and resistance emergence: insights from a modelling study. PLoS Comput. Biol. 10 (4), e1003568. doi:10.1371/journal.pcbi.1003568.

Canini, L., Perelson, A.S., 2014. Viral kinetic modeling: state of the art. J. Pharmacokin. Pharmacodyn. 41 (5), 431–443. doi:10.1007/s10928-014-9363-3.

Cao, P., McCaw, J.M., 2017. The mechanisms for within-host influenza virus control affect model-based assessment and prediction of antiviral treatment. Viruses - Basel 9 (8), 197. doi:10.3390/v9080197.

Chang, S., Zhuang, D., Guo, W., Li, L., Zhang, W., Liu, S., Li, H., Liu, Y., Bao, Z., Han, J., Song, H., Li, J., 2016. The antiviral activity of approved and novel drugs against HIV-1 mutations evaluated under the consideration of dose-response curve slope. PLoS ONE 11 (3), e0149467. doi:10.1371/journal.pone.0149467.

Chanock, R., Finberg, L., 1957. Recovery from infants with respiratory illness of a virus related to chimpanzee coryza agent (CCA) 0.2. Epidemiologic aspects of infection in infants and young children. Am. J. Hyg. 66 (3), 291–300.

Chanock, R., Roizman, B., Myers, R., 1957. Recovery from infants with respiratory illness of a virus related to chimpanzee coryza agent (CCA) 0.1. Isolation, properties and characterization. Am. J. Hyg. 66 (3), 281–290.

Chen, J.J., Chan, P., Paes, B., Mitchell, I., Li, A., Lanctot, K.L., 2015. Serious adverse events in the canadian registry of children receiving palivizumab (CARESS) for respiratory syncytial virus prevention. PLoS ONE 10 (8), e0134711. doi:10.1371/journal.pone.0134711.

Cianci, C., Meanwell, N., Krystal, M., 2005. Antiviral activity and molecular mechanism of an orally active respiratory syncytial virus fusion inhibitor. J. Antimicrob. Chemother. 55 (3), 289–292. doi:10.1093/jac/dkh558.

Collins, P.L., Melero, J.A., 2011. Progress in understanding and controlling respiratory syncytial virus: still crazy after all these years. Virus Res. 162 (1–2), 80–99. doi:10.1016/j.virusres.2011.09.020.

Cox, R., Plemper, R.K., 2016. Structure-guided design of small-molecule therapeutics against RSV disease. Expert Opin. Drug Discov. 11 (6), 543–556. doi:10.1517/17460441.2016.1174212.

Dee, K.U., Hammer, D.A., Shuler, M.L., 1995. A model of the binding, entry, uncoating, and RNA-synthesis of semliki-forest-virus in baby hamster-kidney (BHK-21) cells. Biotech. Bioeng. 46 (5), 485–496. doi:10.1002/bit.260460513.

Dee, K.U., Shuler, M.L., 1997. Mathematical model of the trafficking of acid-dependent enveloped viruses: application to the binding, uptake, and nuclear accumulation of baculovirus. Biotech. Bioeng. 54 (5), 468–490. doi:10.1002/(SICI)1097-0290(19970605)54:5⟨468::AID-BIT7⟩3.0.CO;2-C.

Deming, D.J., Patel, N., McCarthy, M.P., Mishra, L., Shapiro, A.M., Suzich, J., 2013. Potential for palivizumab interference with commercially available antibody-antigen based respiratory syncytial virus diagnostic assays. Ped. Inf. Dis. J. 32 (10), 1144–1146. doi:10.1097/INF.0b013e31829561dd.

DeVincenzo, J.P., McClure, M.W., Symons, J.A., Fathi, H., Westland, C., Chanda, S., Lambkin-Williams, R., Smith, P., Zhang, Q., Beigelman, L., Blatt, L.M., Fry, J., 2015. Activity of oral ALS-008176 in a respiratory syncytial virus challenge study. N. Engl. J. Med. 373 (21), 2048–2058F. doi:10.1056/NEJMoa1413275.

DeVincenzo, J.P., Whitley, R.J., Mackman, R.L., Scaglioni-Weinlich, C., Harrison, L., Farrell, E., McBride, S., Lambkin-Williams, R., Jordan, R., Xin, Y., Ramanathan, S., ORiordan, T., Lewis, S.A., Li, X., Toback, S.L., Lin, S.-L., Chien, J.W., 2014. Oral GS-5806 activity in a respiratory syncytial virus challenge study. N. Engl. J. Med. 371 (8), 711–722. doi:10.1056/NEJMoa1401184.

DeVincenzo, J.P., Wilkinson, T., Vaishnaw, A., Cehelsky, J., Myers, R., Nochur, S., Harrison, L., Meeking, P., Mann, A., Moane, E., Oxford, J., Pareek, R., Moore, R., Walsh, E., Studholme, R., Dorsett, P., Alvarez, R., Lambkin-Williams, R., 2010. Viral load drives disease in humans experimentally infected with respiratory syncytial virus. Am. J. Respir. Crit. Care Med. 182, 1305–1314. doi:10.1164/rccm.201002-02210C.

Dobrovolny, H.M., Baron, M.J., Gieschke, R., Davies, B.E., Jumbe, N.L., Beauchemin, C.A.A., 2010. Exploring cell tropism as a possible contributor to influenza infection severity. PLoS ONE 5 (11), e13811. doi:10.1371/journal.pone.0013811.

Dobrovolny, H.M., Gieschke, R., Davies, B.E., Jumbe, N.L., Beauchemin, C.A.A., 2011. Neuraminidase inhibitors for treatment of human and avian strain influenza: a comparative study. J. Theor. Biol. 269 (1), 234–244. doi:10.1016/j.jtbi.2010.10.017.

Dobrovolny, H.M., Reddy, M.B., Kamal, M.A., Rayner, C.R., Beauchemin, C.A.A., 2013. Assessing mathematical models of influenza infections using features of the immune response. PLoS One 8 (2), e57088. doi:10.1371/journal.pone.0057088.

Eftimie, R., Gillard, J.J., Cantrell, D.A., 2016. Mathematical models for immunology: current state of the art and future research directions. Bull. Math. Biol. 78 (10), 2091–2134. doi:10.1007/s11538-016-0214-9.

Feng, S., Hong, D., Wang, B., Zheng, X., Miao, K., Wang, L., Yun, H., Gao, L., Zhao, S., Shen, H.C., 2015. Discovery of imidazopyridine derivatives as highly potent respiratory syncytial virus fusion inhibitors. ACS Med. Chem. Lett. 6 (3), 359–362. doi:10.1021/acsmedchemlett.5b00008.

Forbes, M.L., Kumar, V.R., Yogev, R., Wu, X., Robbie, G.J., Ambrose, C.S., 2014. Serum palivizumab level is associated with decreased severity of respiratory syncytial virus disease in high-risk infants. Hum. Vaccines Immunother. 10 (10), 2789–2794. doi:10.4161/hv.29635.

Frogel, M., Nerwen, C., Cohen, A., VanVeldhuisen, P., Harrington, M., Boron, M., 2008. Prevention of hospitalization due to respiratory syncytial virus: results from the palivizumab outcomes registry. J. Perinatol. 28 (7), 511–517. doi:10.1038/jp.2008.28.

Gonzalez, D., Schmidt, S., Derendorf, H., 2013. Importance of relating efficacy measures to unbound drug concentrations for anti-infective agents. Clin. Microbiol. Rev. 26 (2), 274–288. doi:10.1128/CMR.00092-12.

González-Parra, G., De Ridder, F., Huntjens, D., Roymans, D., Ispas, G., Dobrovolny, H.M., 2018. A comparison of RSV and influenza in vitro kinetic parameters. PLoS One 13 (2), e0192645. doi:10.1371/journal.pone.0192645.

González-Parra, G., Dobrovolny, H.M., 2015. Assessing uncertainty in A2 respiratory syncytial virus viral dynamics. Comput. Math. Methods Med. 2015, 567589. doi:10.1155/2015/567589.

Graham, B.S., 2011. Biological challenges and technological opportunities for respiratory syncytial virus vaccine development. Immunol. Rev. 239, 149–166. doi:10.1111/j.1600-065X.2010.00972.x.

Groothuis, J.R., Simoes, E., Levin, M.J., Hall, C.B., Long, C.E., Rodriguez, W.J., Arrobio, J., Meissner, H.C., Fulton, D.R., Welliver, R.C., Tristram, D.A., Siber, G.R., Prince, G.A., Vanraden, M., Hemming, V.G., 1993. Prophylactic administration of respiratory syncytial virus immune globulin to high-risk infants and young children. N. Engl. J. Med. 329 (21), 1524–1530. doi:10.1056/NEJM199311183292102.

Gutfraind, A., Galvani, A.P., Meyers, L.A., 2015. Efficacy and optimization of palivizumab injection regimens against respiratory syncytial virus infection. JAMA Pediatr. 189 (4), 341–348. doi:10.1001/jamapediatrics.2014.3804.

Hayden, R.T., Gu, Z., Sam, S.S., Sun, Y., Tang, L., Pounds, S., Caliendo, A.M., 2015. Comparative evaluation of three commercial quantitative cytomegalovirus standards by use of digital and real-time PCR. J. Clin. Microbiol. 53 (5), 1500–1505. doi:10.1128/JCM.03375-14.

Hazen, R., Lanier, E.R., 2003. Relative anti-HIV-1 efficacy of lamivudine and emtricitabine in vitro is dependent on cell type. J. Acq. Immune Defic. Syndr. 32 (3), 255–258. doi:10.1097/00126334-200303010-00003.

Heldt, F.S., Frensing, T., Pflugmacher, A., Gropler, R., Peschel, B., Reichl, U., 2013. Multiscale modeling of influenza a virus infection supports the development of direct-acting antivirals. PLoS Comput. Biol. 9 (11), e1003372. doi:10.1371/journal.pcbi.1003372.

Hoffman, N.G., Cook, L., Atienza, E.E., Limaye, A.P., Jerome, K.R., 2008. Marked variability of BK virus load measurement using quantitative real-time PCR among commonly used assays. J. Clin. Microbiol. 46 (8), 2671–2680. doi:10.1128/JCM.00258-08.

Holder, B.P., Beauchemin, C.A.A., 2011. Exploring the effect of biological delays in kinetic models of influenza within a host or cell culture. BMC Public Health 11 (S1), S10. doi:10.1186/1471-2458-11-S1-S10.

Holford, N.H.G., Sheiner, L.B., 1981. Understanding the dose-effect relationship: clinical application of pharmacokinetic-pharmacodynamic models. Clin. Pharmacokinet. 6 (6), 429–453.

Hu, J., Robinson, J.L., 2010. Treatment of respiratory syncytial virus with palivizumab: a systematic review. World J. Pediatr. 6 (4), 296–300. doi:10.1007/s12519-010-0230-z.

Ispas, G., Koul, A., Verbeeck, J., Sheehan, J., Sanders-Beer, B., Roymans, D., Andries, K., Rouan, M.-C., De Jonghe, S., Bonfanti, J.-F., Vanstockem, M., Simmen, K., Verloes, R., 2015. Antiviral activity of TMC353121, a respiratory syncytial virus (RSV) fusion inhibitor, in a non-human primate model. PLoS One 10 (5), e0126959. doi:10.1371/journal.pone.0126959.

Jones, B.G., Sealy, R.E., Rudraraju, R., Traina-Dorge, V.L., Finneyfrock, B., Cook, A., Takimoto, T., Portner, A., Hurwitz, J.L., 2012. Sendai virus-based RSV vaccine protects African green monkeys from RSV infection. Vaccine 30 (5), 959–968. doi:10.1016/j.vaccine.2011.11.046.

Kahn, J.P., Bartlett, J.G., Bernard, H.R., Bloom, F.E., Greene, W.C., Griffin, D.E., Harlow, E.E., Kaplan, J.R., Landi, M.S., Murphy, F.A., Sapolsky, R., Terry, S., Altevogt, B.M., Shelton-Davenport, M.K., Pankevich, D.E., Taylor, L.K., Repace, A.R., Pope, A.M., Sharples, F.E., 2011. Comparison of immunity to pathogens in humans, chimpanzees, and macaques. In: Chimpanzees in Biomedical and Behavioral research: Assessing the Necessity. National Academies Press, pp. 91–165.

Kakizoe, Y., Nakaoka, S., Beauchemin, C.A.A., Morita, S., Mori, H., Igarashi, T., Aihara, K., Miura, T., Iwami, S., 2015. A method to determine the duration of the eclipse phase for in vitro infection with a highly pathogenic SHIV strain. Sci. Rep. 5, 10371. doi:10.1038/srep10371.

Kakuk, T.J., Soike, K., Brideau, R.J., Zaya, R.M., Cole, S.L., Zhang, J.Y., Roberts, E.D., Wells, P.A., Wathen, M.W., 1993. A human respiratory syncytial virus (RSV) primate model of enhanced pulmonary pathology induced with a formalin-inactivated RSV vaccine but not a recombinant FG subunit vaccine. J. Infect. Dis. 167 (3), 553–561.

Kwanten, L., De Clerck, B., Roymans, D., 2013. A fluorescence-based high-throughput antiviral compound screening assay against respiratory syncytial virus. Methods Mol. Biol. 1030, 337–344. doi:10.1007/978-1-62703-484-5_26.

LaBarre, D.D., Lowy, R.J., 2001. Improvements in methods for calculating virus titer estimates from $TCID_{50}$ and plaque assays. J. Virol. Methods 96 (2), 107–126. doi:10.1016/S0166-0934(01)00316-0.

Leary, J.J., Wittrock, R., Sarisky, R.T., Weinberg, A., Levin, M.J., 2002. Susceptibilities of herpes simplex viruses to penciclovir and acyclovir in eight cell lines. Antimicrob. Agents Chemother. 46 (3), 762–768. 0.1128/AAC.46.3.762768.2002

Liao, L.E., Kowal, S., Cardenas, D.A., Beauchemin, C.A.A., 2017. Exploring virus release as a bottleneck for the spread of influenza a virus infection in vitro and the implications for antiviral therapy with neuraminidase inhibitors. PLoS One 12 (8), e0183621. doi:10.1371/journal.pone.0183621.

Lou, J., Smith, R.J., 2011. Modelling the effects of adherence to the HIV fusion inhibitor enfuvirtide. J. Theor. Biol. 268 (1), 1–13. doi:10.1016/j.jtbi.2010.09.039.

Lundin, A., Bergstrom, T., Bendrioua, L., Kann, N., Adamiak, B., Trybala, E., 2010. Two novel fusion inhibitors of human respiratory syncytial virus. Antivir. Res. 88 (3), 317–324. doi:10.1016/j.antiviral.2010.10.004.

Lundin, A., Bergstrom, T., Trybala, E., 2013. Screening and evaluation of anti-respiratory syncytial virus compounds in cultured cells. Methods Mol. Biol. 1030, 345–363. doi:10.1007/978-1-62703-484-5_27.

Mackman, R.L., Sangi, M., Sperandio, D., Parrish, J.P., Eisenberg, E., Perron, M., Hui, H., Zhang, L., Siegel, D., Yang, H., Saunders, O., Boojamra, C., Lee, G., Samuel, D., Babaoglu, K., Carey, A., Gilbert, B.E., Piedra, P.A., Strickley, R., Iwata, Q., Hayes, J., Stray, K., Kinkade, A., Theodore, D., Jordan, R., Desai, M., Cihlar, T., 2015. Discovery of an oral respiratory syncytial virus (RSV) fusion inhibitor (GS-5806) and clinical proof of concept in a human RSV challenge study. J. Med. Chem. 58 (4), 1630–1643. doi:10.1021/jm5017768.

Marcelin, J.R., Wilson, J.W., Razonable, R.R., 2014. Oral ribavirin therapy for respiratory syncytial virus infections in moderately to severely immunocompromised patients. Transpl. Infect. Dis. 16 (2), 242–250. doi:10.1111/tid.12194.

Miao, H., Xia, X., Perelson, A.S., Wu, H., 2011. On identifiability of nonlinear ODE models and applications in viral dynamics. SIAM Rev. 53 (1), 3–39. doi:10.1137/090757009.

Molinos-Quintana, A., Soto, C.P.-D., Gomez-Rosa, M., Perez-Simon, J.A., Perez-Hurtado, J.M., 2013. Intravenous ribavirin for respiratory syncytial viral infections in pediatric hematopoietic SCT recipients. Bone Marrow Transpl. 48 (2), 265–268. doi:10.1038/bmt.2012.134.

Neumann, A.U., Lam, N.P., Dahari, H., Gretch, D.R., Wiley, T.E., Layden, T.J., Perelson, A.S., 1998. Hepatitis c viral dynamics in vivo and the antiviral efficacy of interferon-α therapy. Science 282, 103–107.

Olszewska, W., Ispas, G., Schnoeller, C., Sawant, D., Van de Casteele, T., Nauwelaers, D., Van Kerckhove, B., Roymans, D., De Meulder, M., Rouan, M.C., Van Remoortere, P., Bonfanti, J.F., Van Velsen, F., Koul, A., Vanstockem, M., Andries, K., Sowinski, P., Wang, B., Openshaw, P., Verloes, R., 2011. Antiviral and lung protective activity of a novel respiratory syncytial virus fusion inhibitor in a mouse model. Eur. Respir. J. 38 (2), 401–408. doi:10.1183/09031936.00005610.

Paes, B., Manzoni, P., 2011. Special populations: do we need evidence from randomized controlled trials to support the need for respiratory syncytial virus prophylaxis? Early Hum. Dev. 87, S55–S58. doi:10.1016/j.earlhumdev.2011.01.012.

Paradis, E.G., Pinilla, L.T., Holder, B.P., Abed, Y., Boivin, G., Beauchemin, C.A.A., 2015. Impact of the H275Y and I223V mutations in the neuraminidase of the 2009 pandemic influenza virus in vitro and evaluating experimental reproducibility. PLoS One 10 (5), e0126115. doi:10.1371/journal.pone.0126115.

Pawelek, K.A., Huynh, G.T., Quinlivan, M., Cullinane, A., Rong, L., Perelson, A.S., 2012. Modeling within-host dynamics of influenza virus infection including immune responses. PLoS Comput. Biol. 8 (6), e1002588. doi:10.1371/journal.pcbi.1002588.

Perelson, A.S., Rong, L., Hayden, F.G., 2012. Combination antiviral therapy for influenza: predictions from modeling of human infections. J. Infect. Dis. 205, 1642–1645. doi:10.1093/infdis/jis265.

Perron, M., Stray, K., Kinkade, A., Theodore, D., Lee, G., Eisenberg, E., Sangi, M., Gilbert, B.E., Jordan, R., Piedra, P.A., Toms, G.L., Mackman, R., Cihlar, T., 2016. GS-5806 Inhibits a broad range of respiratory syncytial virus clinical isolates by blocking the virus-cell fusion process. Antimicrob. Agents Chemother. 60 (3), 1264–1273. doi:10.1128/AAC.01497-15.

Pinilla, L.T., Holder, B.P., Abed, Y., Boivin, G., Beauchemin, C.A.A., 2012. The H275Y neuraminidase mutation of the pandemic a/H1N1 influenza virus lengthens the eclipse phase and reduces viral output of infected cells, potentially compromising fitness in ferrets. J. Virol. 86 (19), 10651–10660. doi:10.1128/JVI.07244-11.

Plant, H., Stacey, C., Tiong-Yip, C.-L., Walsh, J., Yu, Q., Rich, K., 2015. High-throughput hit screening cascade to identify respiratory syncytial virus (RSV) inhibitors. J. Biomol. Screen. 20 (5), 597–605. doi:10.1177/1087057115569428.

Rodriguez, W.J., Gruber, W.C., Groothuis, J.R., Simoes, E., Rosas, A.J., Lepow, M., Kramer, A., Hemming, V., Kim, H.W., Arrobio, J., Milburn, C., Baker, J., Bender, P., Satterwhite, P., Steele, L., King, S., Levin, M., Hensen, S., Aronoff, S., Baer, L., Sanchez, J., Top, F.H., 1997. Respiratory syncytial virus immune globulin treatment of RSV lower respiratory tract infection in previously healthy children. Pediatrics 100 (6), 937–942. doi:10.1542/peds.100.6.937.

Rouan, M.-C., Gevers, T., Roymans, D., de Zwart, L., Nauwelaers, D., De Meulder, M., van Remoortere, P., Vanstockem, M., Koul, A., Simmen, K., Andries, K., 2010. Pharmacokinetics-pharmacodynamics of a respiratory syncytial virus fusion inhibitor in the cotton rat model. Antimicrob. Agents Chemother. 54 (11), 4534–4539. doi:10.1128/AAC.00643-10.

Roymans, D., De Bondt, H.L., Arnoult, E., Geluykens, P., Gevers, T., Van Ginderen, M., Verheyen, N., Kim, H., Willebrords, R., Bonfanti, J.-F., Bruinzeel, W., Cummings, M.D., van Vlijmen, H., Andries, K., 2010. Binding of a potent small-molecule inhibitor of six-helix bundle formation requires interactions with both heptad-repeats of the RSV fusion protein. Proc. Natl. Acad. Sci. USA 107 (1), 308–313. doi:10.1073/pnas.0910108106.

Saez-Llorens, X., Moreno, M.T., Ramilo, O., Sanchez, P.J., Top, F.H., Connor, E.M., 2004. Safety and pharmacokinetics of palivizumab therapy in children hospitalized with respiratory syncytial virus infection. Pediatr. Inf. Dis. J. 23 (8), 707–712. doi:10.1097/01.inf.0000133165.85909.08.

Sampah, M.E.S., Shen, L., Jilek, B.L., Siliciano, R.F., 2011. Dose-response curve slope is a missing dimension in the analysis of HIV-1 drug resistance. Proc. Natl. Acad. Sci. USA 108 (18), 7613–7618. doi:10.1073/pnas.1018360108.

Schelker, M., Mair, C.M., Jolmes, F., Welke, R.-W., Klipp, E., Herrmann, A., Flottmann, M., Sieben, C., 2016. Viral RNA degradation and diffusion act as a bottleneck for the influenza a virus infection efficiency. PLoS Comput. Biol. 12 (10), e1005075. doi:10.1371/journal.pcbi.1005075.

Sedlak, R.H., Nguyen, T., Palileo, I., Jerome, K.R., Kuypersa, J., 2017. Superiority of digital reverse transcription-PCR (RT-PCR) over real-time RT-PCR for quantitation of highly divergent human rhinoviruses. J. Clin. Microbiol. 55 (2), 442–449. doi:10.1128/JCM.01970-16.

Sidorenko, Y., Reichl, U., 2004. Structured model of influenza virus replication in MDCK cells. Biotech. Bioeng. 88 (1), 1–14. doi:10.1002/bit.20096.

Smee, D.F., Wandersee, M.K., Bailey, K.W., Wong, M.-H., Chu, C.K., Gadthula, S., Sidwell, R.W., 2007. Cell line dependency for antiviral activity and in vivo efficacy of n-methanocarbathymidine against orthopoxvirus infections in mice. Antiviral Res. 73, 69–77. doi:10.1016/j.antiviral.2006.04.010.

Smith, A.M., Adler, F.R., Perelson, A.S., 2010. An accurate two-phase approximate solution to an acute viral infection model. J. Math. Biol. 60 (5), 711–726. doi:10.1007/s00285-009-0281-8.

Ståhle, E.L., Schloss, L., Sundqvist, V.-A., Brytting, M., Hökeberg, I., Cox, S., Wahren, B., Linde, A., 1998. Solid phase ELISA for determination of the virus dose dependant sensitivity of human cytomegalovirus to antiviral drugs in vitro. Antivir. Res. 40, 105–112.

Sun, Z., Pan, Y., Jiang, S., Lu, L., 2013. Respiratory syncytial virus entry inhibitors targeting the F protein. Viruses 5 (1), 211–225. doi:10.3390/v5010211.

Taylor, G., 2017. Animal models of respiratory syncytial virus infection. Vaccine 35 (3), 469–480. doi:10.1016/j.vaccine.2016.11.054.

Turner, T.L., Kopp, B.T., Paul, G., Landgrave, L.C., Hayes Jr, D., Thompson, R., 2014. Respiratory syncytial virus: current and emerging treatment options. Clinicoecon. Outcome Res. 6, 217–225. doi:10.2147/CEOR.S60710.

Randolph, A.G., 2007. Ribavirin for respiratory syncytial virus infection of the lower respiratory tract in infants and young children. Cochrane. Database Syst. Rev. 1, CD000181. doi:10.1002/14651858.CD000181.pub3.

Weinberg, A., Leary, J.J., Sarisky, R.T., Levin, M.J., 2007. Factors that affect in vitro measurement of the susceptibility of herpes simplex virus to nucleoside analogues. J. Clin. Virol. 38 (2), 139–145. doi:10.1016/j.jcv.2006.08.023.

Weiss, J.N., 1997. The hill equation revisited: uses and misuses. FASEB J. 11 (11), 835–841.

Weiss, W.J., Murphy, T., Lynch, M.E., Frye, J., Buklan, A., Gray, B., Lenoy, E., Mitelman, S., O'Connell, J., Quartuccio, S., Huntley, C., 2003. Inhalation efficacy of RFI-641 in an African green monkey model of RSV infection. J. Med. Primatol. 32 (2), 82–88. doi:10.1034/j.1600-0684.2003.00014.x.

Wildum, S., Paulsen, D., Thede, K., Ruebsamen-Schaeff, H., Zimmermann, H., 2013. In vitro and in vivo activities of AIC292, a novel HIV-1 nonnucleoside reverse transcriptase inhibitor. Antimicrob. Agents Chemother. 57 (11), 5320–5329. doi:10.1128/AAC.01377-13.

Wright, M., Piedimonte, G., 2011. Respiratory syncytial virus prevention and therapy: past, present, and future. Ped. Pulmonol. 46, 324–347. doi:10.1002/ppul.21377.

Xiao, Y., Miao, H., Tang, S., Wu, H., 2013. Modeling antiretroviral drug responses for HIV-1 infected patients using differential equation models. Adv. Drug Del. Rev. 65 (7), 940–953. doi:10.1016/j.addr.2013.04.005.

Yan, D., Lee, S., Thakkar, V.D., Luo, M., Moore, M.L., Plemper, R.K., 2014. Cross-resistance mechanism of respiratory syncytial virus against structurally diverse entry inhibitors. Proc. Natl. Acad. Sci. USA 111 (33), E3441–E3449. doi:10.1073/pnas.1405198111.

Zheng, X., Wang, L., Wang, B., Miao, K., Xiang, K., Feng, S., Gao, L., Shen, H.C., Yun, H., 2016. Discovery of piperazinylquinoline derivatives as novel respiratory syncytial virus fusion inhibitors. ACS Med. Chem. Lett. 7 (6), 558–562. doi:10.1021/acsmedchemlett.5b00234.